Lunds Universitets Naturgeografiska Institution

Seminarieuppsatser Nr. 38

Desertification mapping of Horqin Sandy Land, Inner Mongolia, by means of remote sensing

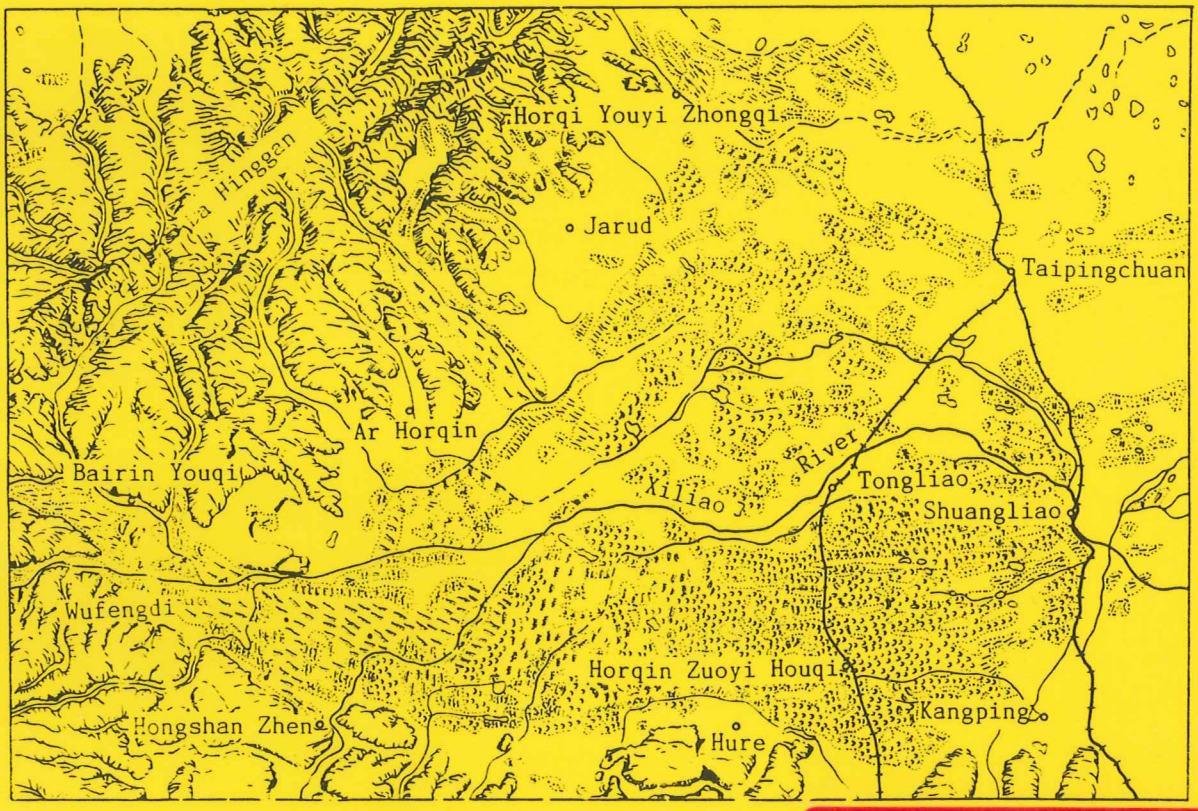

Patrik Bremborg

Department of Physical Geography,
Lund University
Sölvegatan 13, S-221 00 Lund,
Sweden

1996

Lunds Universitets Naturgeografiska Institution

Seminarieuppsatser Nr. 38

Desertification mapping of Horqin Sandy Land, Inner Mongolia, by means of remote sensing

Patrik Bremborg

Department of Physical Geography,
Lund University
Sölvegatan 13, S-221 00 Lund,
Sweden

1996

CONTENTS

ABSTRACT

The extent of today's land degradation and desertification in the arid, semi-arid, and sub humid regions of China is a serious threat to the social and economic development in these areas. A national programme for monitoring and classification of drylands has been implemented by the Chinese Academy of Science. Areas are classified into degrees of desertification on the basis of vegetation cover, biomass change, deflation, and deposition. This study evaluates the use of Landsat MSS derived vegetation indices for desertification mapping as an alternative to the labour intensive field measurements used in the currently used classification system. Ratio-, difference-, normalized-, and soil adjusted vegetation indices images, together with MSS band 6, the first principal component, and maximum likelihood classified images are used and compared. Accuracy is evaluated using a thematic desertification map of Horqin Sandy Land, Inner Mongolia (1991), compiled by the Lanzhou Institute of Desert Research, Chinese Academy of Science, for validation. The green vegetation cover estimates images all showed comparable results, and no one stood out as superior to the others. Total accuracy is approximately 48% for all indices, while mean accuracy varies between 26.8% and 64.1%for individual classes. Annual plants are theorised to be the cause of the class confusion, hence the low accuracy.

1. INTRODUCTION

During the fall of 1995 as I was about to sum up my years at the Department of Physical Geography, at Lund University, with a Master's thesis, I was introduced to a research project dealing with the semi-arid regions of northern China. The project appealed to me, and my supervisor Ulf Helldén gave me some literature on the on-going debate on land degradation and desertification. As I decided to complete my thesis as a first step to more in-depth studies, I was given some more literature, maps and satellite images over the western part of Horqin Grassland in Inner Mongolia, northeastern China. The material included a thematic map of the Horqin Grassland, showing land parcels divided into four *degrees of desertification*. A classification scheme based on multiple criteria had been constructed by the Chinese Academy of Science for mapping purpose. I was curious to discover whether it was possible to use Landsat MSS data to classify an image over the same area as the map in the four desertification degrees, using only 1 criteria; vegetation cover estimates. I opted to use and test different vegetation indices against each other in the classification scheme. My goal, therefore, was to find a short-cut following a rather simple classification procedure, to the more rigorous classification scheme used in compiling the desertification map, not simply to achieve as good a classification as possible.

The study is thus a methodological one, and most effort has been put on the theoretical background and the evaluation of the classifications derived from the vegetation indices.

1.1 AIM OF THE STUDY

This study involves the application of remote sensing methodologies in developing a land cover mapping scheme for the western Horqin Sandy Land in Inner Mongolia, China. It represents an introductory step leading to a more comprehensive study of the regions of northeastern China.

The principal aim of the study is to explore and evaluate different approaches to vegetation green cover estimation, by means of remote sensing, in an effort to find an easy and efficient method to classify vegetation cover into desertification degree classes in accordance with the Chinese academy of science classification system (see section 1.4). If

successful, it would enable continuous monitoring on a yearly basis, rather than on a decadal base as is now the case.

1.2 BACKGROUND

The Chinese semi-arid steppe ecosystem has been subject to direct human manipulation two to three thousand years (Dregne, 1983), but the scale and extent of today's land degradation is without parallel. Nutritionally stressed livestock, degraded vegetation, and water and wind eroded range-, and cropland all indicate a decline in the land's agricultural production. The present desertification trend owes its cause to the adverse agricultural production practices that are associated with overriding socio-economic and political agendas (Sheeny, 1992). A low awareness of the severity of the current situation amongst the government prohibits any rapid solution as long as no convincing practical policies are formulated.

Mei (1985) in studying the Horqin Sandy Land in the northeastern Inner Mongolia concluded that the main cause of the current desertification problem in the semi-arid steppe grazing lands is the land-use shift from highly productive grazing land to marginal farmland adjacent to rivers and villages, overgrazing by livestock, cultivation of formerly stabilized sand dunes, and conversion of loess uplands to rainfed farming.

The meteorological record of the last half century showing decreasing annual rainfall in the province (Zhu *et al.*, 1988a) is in no way promising for the struggle to overcome the increasingly acute land degradation.

The literature reveals different trends in land degradation/desertification processes over the years. The 1950s to 70s period was characterised by loss of total land productivity due to the development of severely desertified land from already moderately desertified land. The land degradation process in the recent decade has been characterised by serious wind erosion in newly reclaimed land and range-land due to over-cultivation, over-grazing, fuelwood gathering, and misuse of water resources (Walker, 1982; Wang and Imagawa; Zhu and Liu, 1983; Zhu *et al.*, 1988a; Zhu and Wang, 1990).

Desertification is considered a major problem for economic development and environmental protection in northern China and improved methods for monitoring and assessing the current status and trends is required if the national programme for combating desertification is to obtain satisfactory results (Walls, 1982; Wang and Imagawa; Zhu and Liu, 1983)

To better understand the processes at hand, a national research project was implemented under the direction of professor Zhu Zhenda in the early 1980's. One of the objectives was to put forth principles and methods for compiling maps of the status or degree of desertification in China, to allow for continuous monitoring of arid, semi-arid, and sub-humid regions. A scheme for classifying the status of the land into degrees of desertification based on multiple criteria was set up, dividing the degree of severity into four classes (Wang and Imagawa; Zhu and Liu, 1983; Zhu, 1984; Zhu *et al.*, 1988b). The word desertification, rather than land degradation, will be used throughout this paper, as it is the word most commonly used in the Chinese literature available in English. The word desertification is used with the same definition adopted by the UN (1977), and UNEP (1984), and most recently, Agenda 21 at the 1992 UN Conference on Environment and Development (UNCED). That is: *...land degradation in arid, semi-arid and dry sub-humid areas resulting from various factors, including climatic variations and human activities.*

1.3 STUDY AREA

Horqin Steppe, also called Horqin Grassland, is situated in the western part of the Northeastern Plains in the eastern Inner Mongolia (41°41'40''- 47°39'20''N, and 116°21'30''- 126°14'46''E). It is one of the largest and most important range-land areas in China. The Horqin Sandy Land (the area studied here) is the arid to semi-arid area of the Horqin Grassland region. It mainly comprises the alluvial plains of the Xiliao River and its tributaries southeast of the Da Hinggan Ling (Great Hinggan mountain ranges) and to the north of the Liaoning mountains and loess hills. Figure 1 shows the study area delineated on a sketch map typically used in Chinese reports and papers (Zhu *et al.* 1988a).

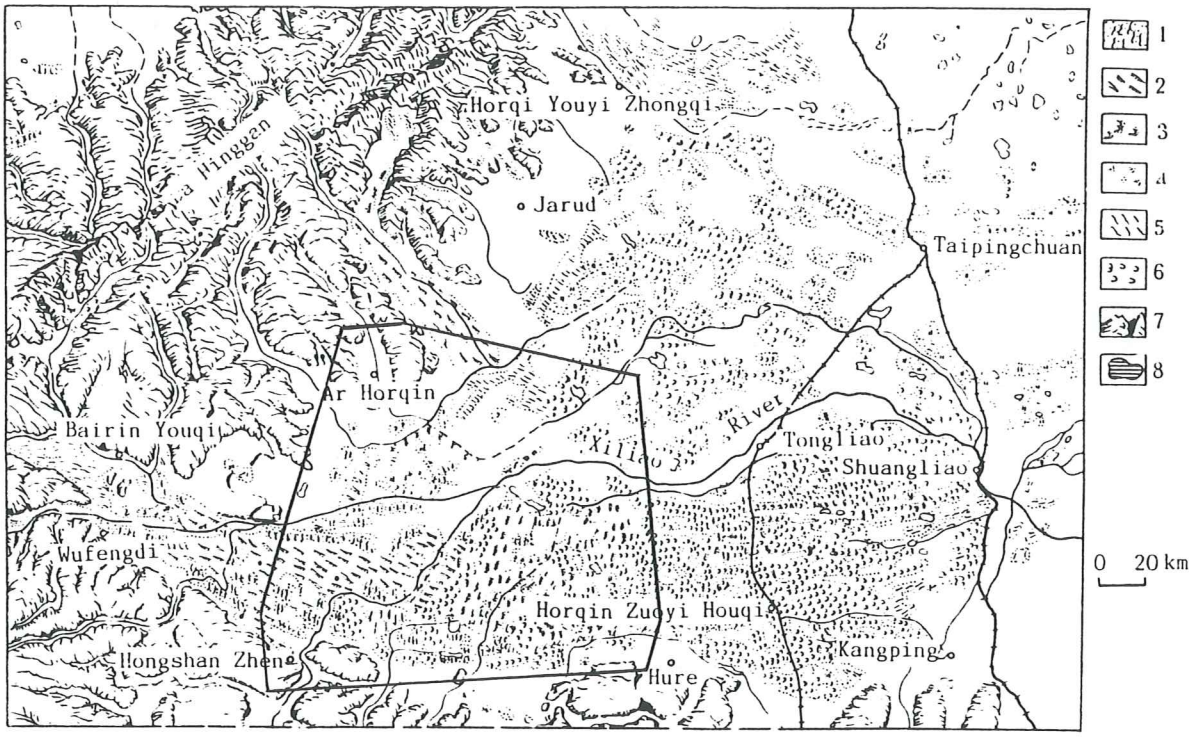

Figure 1. Sketch map of Horqin sandy Land (from Zhu *et al.* 1988a), with an approximate outline of the area studied with Landsat data. Classes: 1. mobile barchan dunes and sand ridges, 2. semi fixed longitudinal dunes, 3. semi fixed honeycomb dunes and sand ridges, 4. semi fixed bush vegetated dunes, 5. fixed longitudinal dunes, 6. fixed honeycomb dunes on sand ridges, 7. mountains and hills, 8. lakes.

The area belongs to the continental monsoon climate, and lies in the transitional zone between the semi-arid and sub-humid zones. Relative proximity to the ocean and the influence of the summer monsoon brings copious amounts precipitation in Horqin Sandy Lands compared to many of the other desertification prone areas in China. The annual precipitation is in the range 315 - 490 mm, and the annual evaporation is 1800 mm. The precipitation is primarily controlled by the southeast summer monsoon, and its regional distribution controlled by topography. Most rain falls in the summer, often in the form of erratic thunderstorms and conventional fronts, with July and August accounting for 70 per cent of the annual total. Winters are cold and windy. The prevailing wind direction, controlled by the Siberian anticyclone, is northwest. Strong winds that causes dust storms and dust devils occur mainly from March through May, (Zhu *et al.* 1986, Zhu *et al.* 1988). This very unfortunate meteorological feature means that the end of the dry season coincides with the most windy season.

1.4 THE DESERTIFICATION MAP OF HORQIN SANDY LAND, AND THE DESERTIFICATION DEGREE CLASSIFICATION SYSTEM

One objective of the national programme "Combating Desertification in China" is to repeatedly monitor the north China drylands, in order to identify regions at risk as well as identifying areas of change. This phase of the programme included the compilation of the so called desertification maps. The first step was to select the case study areas from the arid to semi-arid steppe in north China. Twelve areas, together covering 500,000 sq. km, were mapped in scale 1:350,000 or 1:500,000 according to the following classification scheme; latent, slight, moderate, and severe. The mapping is based on (i) visual image interpretation of aerial photographs and satellite images, (ii) evaluation of physical and socio-economic data, and (iii) field monitoring and investigations. A robust classification system, not influenced by local variability of data availability, but based on strictly defined criteria was constructed. This prerequisite, together with the fact that most affected areas are subject to aeolian activities, formed a classification scheme based on the four criteria in table 1 (Wang and Imagawa).

Table 1. Criteria for sandy desertification used in compiling the desertification mapping of north China (source: Wang and Imagawa). * *Biomass decline is measured in comparison to control plots with known biomass.*

	Vegetation cover (%)	Biomass decline (%)*	Area of wind erosion/deposition per unit area (%)	Spread of wind erosion /deposition per unit area and year (%)
Latent	> 60 %	<1.5	<5	<1
Slight	60-30	1.5-3.5	5-25	1-2
Moderate	30-10	3.5-7.5	25-50	2-5
Severe	< 10	>7.5	>50	>5

From an inventory standpoint, the most accessible studied criterion in the classification scheme is the vegetation cover. Vegetation cover is also the heaviest weighted variable (Zhao, pers. com.; Zhu and Liu, 1983). Zhu *et al.* (1988a) describes typical vegetation status within the different desertification degree classes. Latent desertified land is characterised by dense, mostly perennial, vegetation and unaffected topsoil. A great variety of plant species that may be used for livestock fodder flourish here. Typical species are *Artemisia halodendron, Caragana microphylla,* and *Hedysarum fruticosum*. The slightly desertified land resembles the latent class but with a less dense complement of perennial species such as *A. halodendron, and C. microphylla*. In the moderate desertified

class, vegetation density decreases relative to the former. The annual variation is great, with 60 to 70 per cent of the fresh biomass accounted for by annual plants, such as *Setaria viridis*, which blooms in July and August. In April, however, the land revèrts to shifting sand dunes. The average plant cover is 20 to 30 per cent. The severely desertified land has lost all its utilisation value. Vegetation cover is less than 10 per cent, and plants are found scattered on the dunes and in the inter dune depressions. Species include *Agriophyllum squarrosum,* and *Salix gorgejevii.*

The map used in this study is the "Map of Land Desertification in Horqin Grassland, 1:500,000", (Lanzhou Institute of Desert Research, Academia Sinica, 1991. Chengdu Cartographic Publishing House). Both a digitised version and a hard copy of the map was used in the study in identifying class-typical areas for the computer aided interpretation of the images, and for the final evaluation of the classification result.

An older desertification map, from the early 1980's (Zhao, pers. com) was to aid in the selection of training sites for the automated classification of the satellite image. This older map is probably classified according to the somewhat different criteria given in Zhu and Liu (1983)

2. METHODOLOGICAL BACKGROUND

This section is a review of the theoretical background to the image processing methods used in the study. The methods as applied to this study is presented in section 3, Methodology

2.1 GEOMETRIC CORRECTION

The following description of the geometric correction of satellite data is mainly compiled from Jensen (1985) and Richards (1993). Raw satellite data most often contains geometric distortions. Those distortions that can be corrected through analysis of sensor characteristics and ephemeris include scan skew, mirror-scan velocity nonlinearities, panoramic distortion, spacecraft velocity, and perspective geometry. Errors that can only

be corrected through the use of ground control points (GPC) are sensor system attitude (roll, pitch, and yaw) and/or altitude (Bernstein, 1983). A thorough discussion is given in Richards (1993). The objective of a geometric correction is to render temporal sequences of image data comparable and/or to make that data comparable to a map of any given projection. The latter is referred to as image-to-map rectification or registration.

Landsat MSS data is system corrected. To make the data comparable to the thematic map an image-to-map registration was performed. The method relies upon establishing a mathematical relationship between locations of pixels in an image and the corresponding coordinates of those points on the ground (*i.e.* a map). The approach allows the image analyst to make geometric corrections irrespective of knowledge of the sources and types of distortions.

2.2 IMAGE REGISTRATION USING MAPPING POLYNOMIALS AND GROUND CONTROL POINTS

In establishing an image-to-map relationship, we first define two Cartesian coordinate systems. One describing the position of points on the map (x,y) and the other coordinate system defining the location of pixels in the image (u,v). These two coordinate systems can be related via a pair of mapping functions f and g such that:

$u = f(x,y)$ (forward polynomial)

$v = g(x,y)$ (backward polynomial)

When these function are known, it is possible to locate a point in the image knowing its position on the map. The form of the mapping functions that are not known are usually chosen as simple, first to fourth order, polynomial functions. A second order function be described as:

$$u = a_0 + a_1x + a_2y + a_3xy + a_4x^2 + a_5y^2$$

$$v = b_0 + b_1x + b_2y + b_3xy + b_4x^2 + b_5y^2$$

The coefficients a_i and b_i are unknown, but can be estimated by identifying features in the map, such as road intersections or other prominent landscape features, which can also be identified in the satellite image (GCP's). Enough GCP's must be chosen to fulfill the requirements of the polynomial function used, six in the case of second order function. Considerably more control points than the minimum requirement are, however, used to obtain a reasonable distribution over the whole image. Before the registration is performed, it is necessary to check how well the coefficients derived account for the geometric distortion in the input image. The evaluation used involves computation of a root mean square error (RMS_{error}) for each GCP.

$$RMS_{error} = SQRT((u-x)+(v-y))$$

Those GCP's that exhibit the greatest RMSerror are not included in the analysis. A sum of all RMSerrors are calculated to check that it does not exceed a user specified threshold.

2.3 RESAMPLING OF PIXEL BRIGHTNESS VALUES

The registration takes care of the geometric correction. The next step is to chose a suitable method for brightness value interpolation or resampling. With the nearest neighbour resampling method the brightness value of the pixels closest to the specified input coordinates is assigned to the output coordinate. This method is usually preferred if the image is to be classified as original pixel brightness values are retained (Richards, 1993). The nearest neighbour resampling might result in a somewhat jagged appearance of the image if there is significant rotation or scale change.

2.4 RADIOMETRIC CORRECTION

When image data is recorded by a satellite sensor it may contain errors in the measured brightness values of the pixels. These radiometric errors can result from the actual instrumentation, and from the effect of the atmosphere through which the radiation is transmitted. The atmosphere might alter the true ground reflectance values significantly by scattering and absorption. Absorption by molecules of oxygen, carbon dioxide, ozone and water is a selective process that tends to lower the measured brightness from landscape

measurements (Jensen, 1986). The effects are usually minimised by sensors being designed to operate away from the interfering regions. Scattering is thus the dominant source of radiometric distortion in image data, leading to increases in the brightness measurements. Methods for correcting the influence of the atmosphere have to be taken into consideration for accurate application of the image data. An absolute radiometric calibration is usually not possible, as the computation involves optic, climatic and atmospheric parameters not easily available for any given region at any given time. Therefore the relative calibration method, described by Robinove (1982), Nelson (1985), and Markham and Barker (1986), is usually a more realistic way to covert image data into scientifically meaningful units, such as at-satellite reflectance. Performing a simple haze removal will lower the distortion resulting from scattering (Richards, 1993). These operations also make image data suitable for band-ratioing and multi-temporal studies. Robinove *et al.* (1981) points out that the reflectance equation assumes (i) a Lambertian (diffuse) reflecting surface, and (ii) a flat terrain. The computation is a three-step operation, first involving the conversion of the absolutely calibrated digital numbers to spectral radiance (Lλ), which is accomplished with the equation provided by Markham and Barker 1986):

$$L\lambda = L\min\lambda + \frac{L\max\lambda - L\min\lambda}{DN\max} \times DN$$

where:

DN	=	Digital Number on CCT
DNmax	=	Maximum digital number
*L*minλ	=	Minimum spectral radiance (mW/cm2 sr μm)
*Lmax*λ	=	Maximum spectral radiance (mW/cm2 sr μm)
*L*λ	=	Spectral radiance (mW/cm2 sr μm)

The next step is to adjust for effects of varying sun angle, sun distance and irradiance. Given these parameters and the spectral radiance, we can calculate the more tangible at-satellite reflectance values. These parameters are specific for the sensor and the receiving station. The at-satellite reflectance is calculated in accordance with Markham and Barker (1986):

$$\rho p\lambda = \frac{\pi \times L\lambda \times d^2}{Esun\lambda \times \cos\Theta s}$$

where:

$\rho p\lambda$	=	Unitless effective at-satellite reflectance
$L\lambda$	=	Spectral radiance (mW/cm² sr μm)
d	=	Earth-sun distance in astronomial units (from astronomical almanac)
$Esun\lambda$	=	Mean solar exoatmospheric spectral irradiance (mW/cm² μm)
Θs	=	Solar zenith angle in degrees

The resulting at-satellite reflectance values are then rescaled to a tangible format, i.e. 8 bit data with whole numbers ranging from 0 to 255. Bands are scaled uniformly to retain the inter-band relationship.

A third radiometric preprocessing step might be to perform a haze removal method. There are three approaches to this method. One assumes that the longest waveband is essentially unaffected by atmospheric scattering, and that this band can function as a yardstick to the amount of atmospheric effect to all the band's of the scene at hand (Ahlcrona, 1988; Robinove *et al.*, 1981). Thus the minimum DN value of that band is subtracted from all pixel values in all bands. Another method (Jensen, 1986, and Richards, 1993) is to use each bands minimum value to subtract from each pixel value in that band. A third approach described by Helldén (1984) assumes there are at least two pieces of land with non-changing spectral properties. One dark area, e.g. non vegetated bedrock in shadow, is set to zero, and a light area, e.g. non vegetated quartzitic sand, is set to 255. The data is then linearly stretched.

2.5 SPECTRAL REFLECTANCE OF VEGETATION

The absorption, reflection, and transmission of electromagnetic radiation from green vegetation is dependent upon pigmentation, physiological structure, and water content. In the visible wavelengths, the chlorophyll pigmentation is the major factor affecting the reflectance properties. A large part of the incident radiation is absorbed, especially at approximately 0.45 μm (blue region) and 0.65 μm (red region). In the near infrared, the plant's physiological structure gives rise to the unique spectral reflectance characteristics

of healthy green vegetation. About half the incident energy is reflected, very little is absorbed, and the rest transmitted. In the middle infrared portion of the spectra, water content reduces the reflectance by light absorption. The different characteristics between red and near infrared reflectance provides the basis for most vegetation indices. Figure 2 depicts the reflectance characteristics of vegetation, senescent grass, and green grass.

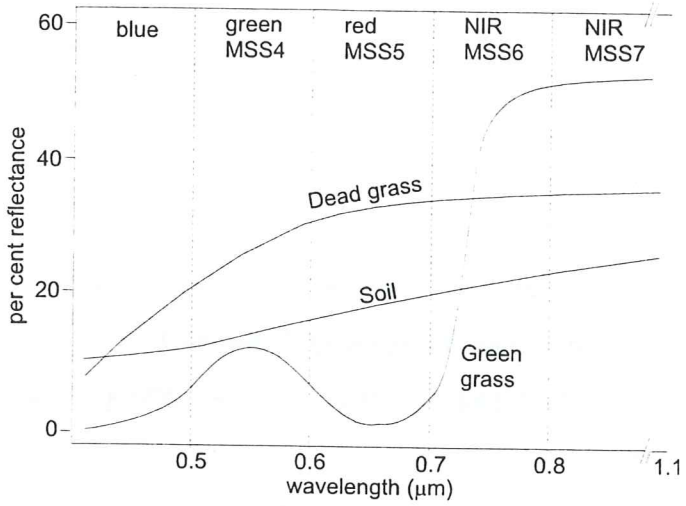

Figure 2. The spectral reflectance characteristics of soil, dead grass, and green grass (modified from Jensen, 1986).

The reflectance does not, however, solely depend on the plant itself, but also depends on the amount of senescent vegetation, soil background properties, sun angle, and canopy geometry. Differences in soil properties and its influence on spectral signatures are thoroughly discussed in Huete (1989). Sun angle and canopy geometry combines to make discrepancies in canopy shadows, that dampens the reflectance in all wavebands. The influence is greater in the visible than in the near infrared wavebands. A band ratio will thus not entirely normalise the amount of shadow (Colwell, 1974). Graetz and Gentle (1982), Otterman and Robinove (1983), and Printer *et al.* (1985) discussed the effect of shadow on reflectance in great detail.

2.6 VEGETATION INDICES

The spectral reflectance characteristics of green vegetation has promoted the development of indices that attempt to enhance the spectral contribution of vegetation while minimising the influence of soil background, solar irradiance, sun angle, senescent vegetation, and atmosphere (Tucker, 1979; Rouse, 1973; Colwell, 1974; Kauth and Thomas, 1976;

Richardson and Wiegand, 1977; Ashley and Rea, 1975). Several vegetation indices have been developed that utilise red- and NIR reflectance in the form of ratios or in linear combinations. More recently a hybrid set of vegetation indices has emergèd. The formulae and notable references of the vegetation indices used in this study are found in Table 2.

Table 2. Red and NIR vegetation index formulae.

NDVI	NDVI = (NIR-Red) / (NIR+Red)	Rouse *et al.*, 1973
RVI	RVI = NIR / Red	Jordan, 1969
DVI	DVI = a × NIR - Red	Tucker, 1979
SAVI	SAVI = (NIR-Red) / (NIR+Red+L) × (1+L)	Huete, 1988

The value of these indices lie in their potential ability to estimate vegetation variables such as percent green cover, leaf area index , productivity, biomass, and absorbed photosynthetically active radiation (Jordan,1969; Colwell, 1974; Tucker, 1979; Hatfield *et al.*, 1985; Asrar *et al.*, 1984; Sellers, 1989).

When remotely sensing vegetation in arid in semi-arid climates, one usually deals with rather sparse vegetation cover. Hence the substrate will have a significant effect in the response of a vegetation index. Different soil properties, such as moisture content, texture, organic matter, iron oxide amount and roughness affect the amplitude rather than the shape of the spectral signatures. In general, increased moisture and iron oxide content, and increased organic matter content dampens the reflectance. Decreased mean particle size and a smoother surface will increase the reflectance. A detailed discussion of the concept is given in Huete (1989). Several indices are designed specifically to minimise this influence of the soil background. Those used in this study are described below. The performance of different vegetation indices and the influence of soil background are thoroughly described in Baret *et al.*, (1989), Elvidge and Lyon (1985), Elvidge and Chen (1995), Graetz and Gentle (1982), Huete (1989), Olsson (1985), and Richardson and Wiegand (1977).

2.6.1 The ratio vegetation index, RVI

A simple ratio of the spectral band recording visible red with that recording near-infrared produces the Ratio Vegetation Index, RVI, and was used by Jordan (1969). Tucker (1979) and Richardson and Wiegand (1977). The latter evaluated this index as an estimator of several different vegetation parameters.

2.6.2 The normalized difference vegetation index, NDVI

One of the oldest and the most used vegetation indices is the Normalized Difference Vegetation Index proposed by Rouse *et al.* (1973), who then called it the Vegetation Index, and also derived a transformed version by adding 0.5 to the index and then taking the square root of the sum. Both indices have shown good correlation with wet biomass and interrelated biophysical parameters (Tucker, 1979) and crop cover (Richardson and Wiegand, 1977). The NDVI normalises the difference between the NIR and the red channels so that the values ranges from -1 to +1. It has also proven effective in normalising soil background spectral variations (Colwell, 1974), and irradiance variations (Tucker, 1979).

An asymptotic behaviour of the NDVI in estimating high green vegetation parameters has been pointed out by several authors (Tucker, 1979; Holben *et al.*, 1980). This means that the NDVI will produce nonlinear, thus erroneous, estimations of high quantities of vegetation.

There is an ongoing debate on the usefulness of the NDVI and what can actually be estimated from it. The literature points out NDVI correlation with the full gamut of vegetational biophysical states as well as biophysical rates. A thorough discussion is given in Sellers (1989).

2.6.3 The difference vegetation index, DVI, and the perpendicular vegetation index, PVI

Kauth and Thomas (1976), in developing their Tassled Cap transformation, found that soil reflectance variation in a multi-dimensional data space formed a plane, and that vegetation lies perpendicular to this soil plane. Richardson and Wiegand (1977) used this concept of

perpendicular distance to the soil line as an indicator of vegetation development. They estimated the soil line equation by linear regression. The more dense the vegetation, the further away from the soil line one would find its corresponding pixel in the red-NIR space. Constant levels of vegetation covering soil with differing characteristics would be found at the same orthogonal distance from the soil line but at different distances from the origin (Fig. 3).

This computationally awkward vegetation index induced Richardson and Wiegand to propose the difference vegetation index (DVI) which achieves the same end. DVI is calculated by subtracting red from NIR multiplied with the slope of the soil line.

2.6.4 The soil adjusted vegetation index, SAVI

Huete (1988) proposed a soil adjusted vegetation index to minimise the influence of soil brightness from red and NIR spectral vegetation indices. Vegetation indices in general rely on the concept of a soil line in the red and NIR reflectance space (fig 3). Variation in soil characteristics, primarily moisture content, is explained by this line. The variation in soil colour, especially red and yellow tones (Kauth and Thomas, 1976), results in a non-parallel secondary axis in the red and NIR space, hindering the detection of very low amounts of vegetation (Huete *et al.*, 1984). Therefore, with a truly varying soil background, the soil line will look more like an elongated oval shape than an actual line. Most soil spectra however, fall on or close to the soil line, making values of bare soil with different conditions, nearly identical for vegetation indices using the concept (Huete, 1988). The variation in vegetation amount is then described by vegetation isolines which explain constant vegetation amount for differing soil characteristics. The ratio-based vegetation indices can be graphically displayed as isolines with increasing slopes diverging out from the origin, while the orthogonal indices' isolines lay parallel to the soil line. Figure 3 shows how a pixel (A) describing a partial vegetation cover over a dry soil would behave if the soil became wet, and the pixel were to conserve its index value. In the case of a ratio vegetation index, the pixel would shift towards the origin to (C), and being a orthogonal based index, it would be bound to shift parallel to the soil line to (B). Huete *et al.* (1985) and Huete and Jackson (1987) used controlled ground measurements to describe soil lines in the red-NIR reflectance space. They found vegetation isolines

occurring in-between those of ration- and orthogonal-based isolines, such as shown by the broad lines in Figure 3.

Huete (1988) thus modelled the NDVI to shift its origin to the empirically derived convergence point (D in Fig. 3). This can be achieved by simply add a constant, L, to the denominator of the NDVI equation. To maintain the bounded conditions (-1 to +1) of the NDVI a multiplication factor (1+L) is needed (Huete, 1988). Huete (1988) concludes that there might be a couple of optimal constant values, depending on if one studies low, intermediate or high vegetation densities. With varying vegetation densities or no prior knowledge of vegetation cover, an adjustment factor of L = 0.5 was shown to substantially reduce soil noise problems.

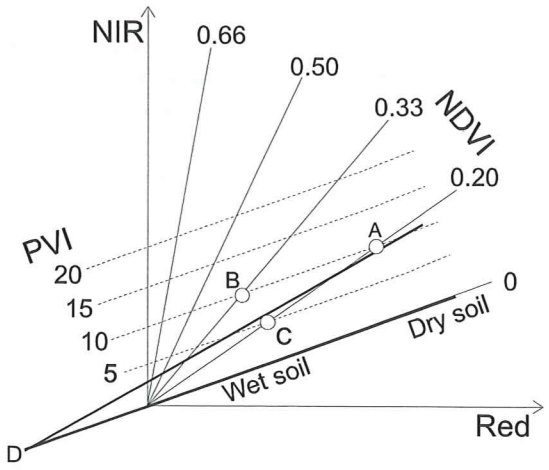

Figure 3. Vegetation spectra isolines in NIR-Red wavelength space as predicted by the Normalized Difference-, and Perpendicular Vegetation Index (Modified from Huete, 1988). For details and description of the figure, see text above.

2.6.5 The principal components analysis, PCA

Principal components analysis of Landsat MSS data has shown results similar to Kauth and Thomas' (1976) Tassled cap transformation in constructing new axes describing vegetational variation (Misra and Wheeler, 1977). The similarities between the two methods are quite remarkable considering that the technique underlying them are quite different. With principal components analysis one does not impose any prior order on the principal directions, as is the case with the Kauth and Thomas approach. PCA successively factors the total variation in the data into mutually orthogonal components, each successively describing the maximum of remaining variation (Jensen, 1986).

Principal component analysis (PCA), also referred to as Karhunen-Loeve or Hotelling transform, has proven to be useful in many aspects of remote sensing. The method transforms raw image data into as many principal components as there are original bands. Each component describing the maximum remaining variance within the data. In the case of MSS data with four bands, the first two components are usually meaningful, but the remaining components are usually left to explain just the noise inherent in the data.

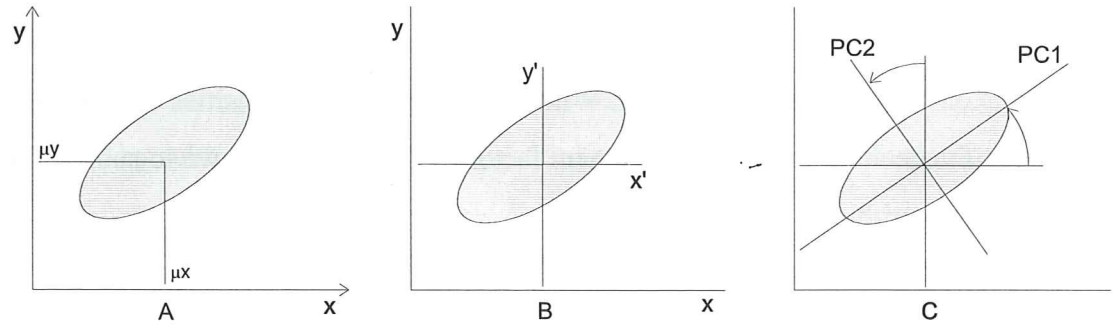

Figure 4. Graphical representation of the spatial relationship between the first principal components. (A) A scatterplot of a two-dimensional data space with the means of the distribution labeled μx and μy. (B) A new coordinate system is created by shifting the axes to the x' and y' system. (C) The x' and y' axes system is then rotated about its origin (μx, μy) so that PC1 is projected through the semimajor axis of the distribution, and that the variance of PC1 is a maximum. PC2 is perpendicular to PC1. The PC axes are the principal components of the two-dimensional data space (modified from Jensen, 1986).

The following description of the principal components is taken from Richards (1993), where more thorough presentation and numerical examples are given.

The principal component analysis (PCA) is performed by applying a transformation to a correlated set of multispectral data, so that we get a new uncorrelated set of data with ordered variance properties. This is accomplished by a translation and rotation of the original coordinate system (Figure 4). In practice, when applying PCA to image data, three basic steps are taken (usually supported within modern image analysis packages). The first is to compute a n x n covariance matrix, where n is the dimensionality of the data set. The second step involves determination of eigenvalues (the diagonal elements of the matrix) and eigenvectors of the covariance matrix. The eigenvalues are used to assess the distribution of data variance over the components. A rapid fall in the magnitude of the eigenvalues indicates a high correlation between the original spectral band data. The final step is to compute the components using the eigenvectors of the covariance matrix as weighting coefficients. The components (eigenvalues) of the eigenvectors act as

coefficients in determining the principal component brightness values for pixels as the weighted sum of its original brightness. The translation and rotation therefore results in a new coordinate system, shown in Figure 4, where the major axis is associated with the maximum amount of variance of the data space. This new axis is called the first principal component (PC1). The second principal component (PC2) is perpendicular (orthogonal) to PC1 and explains the second most variance of the data.

In practical image analysis use of PCA, with Landsat MSS data, it will be noticed that only the first couple of principal components inhabit meaningful information. The last PC's will describe noise inherent in the data, such as striping, speckles or random noise. PCA thus give us a powerful measure in reducing the often redundant information in the well correlated Landsat MSS data. In addition the eigenvalues can be used to determine the percent of total variance explained by each of the principal components (%*p*), using the equation (Jensen, 1986):

$$\%p = \frac{eigenvalue\lambda_p}{\sum_{p=1}^{n} eigenvalue\lambda_p} \times 100$$

It will most often be shown that the first two components describe about 95% of the total variance. What the components represent, or are associated with, can be illustrated by computing the correlation of each band with each component (Jensen,1986).

Byrne *et al.*(1980) and Ingbritsen and Lyon (1985) successfully used PCA in land cover change studies. Walker (1982) used the second PC to describe variation in vegetation when studying deserts in China.

2.7 IMAGE CLASSIFICATION

In order to make use of a supervised classification routine, image data information on the spectral properties of each desired land-cover type must be gathered to allow for calculations of variables crucial for the automated classification process. This information is referred to as training data.

Training data is collected by delineating areas of the desired land cover classes on the image or according to data gathered from ancillary or field data. These areas are chosen to contain as pure signals as possible for each class. One class can be described by several training areas for the same cover type. This might be desired as the same land cover can give rise to non-identical spectral responses throughout the image (Lillesand and Kiefer, 1987). Sufficient training samples for each training class must be collected to fulfill the statistical requirements of the classification algorithm. Richards (1993) states that N+1 samples are needed for an N dimensional multispectral space. It is, however, desirable to have rather large training samples in order to represent the spectral variation for each class. Swain and Davies (1978) recommend that a minimum of 10N samples per training set are used, but strongly endorse 100N if possible. Training areas are usually chosen with some *a priori* knowledge of the area, but can also be chosen on the basis of visual image interpretation.

In this study the maximum likelihood classification algorithm (MLC) was chosen to classify the four original MSS-bands to be compared with the single band classification of the various vegetation indices. The MLC assumes that the classification training data is normally distributed. Under this assumption, the distribution of training data can be described by its mean vector and covariance matrix. Given these parameters the MLC computes the statistical probability of each pixel being a member of a specified class (Lillesand and Kiefer, 1987). The concept is illustrated in figure 5.

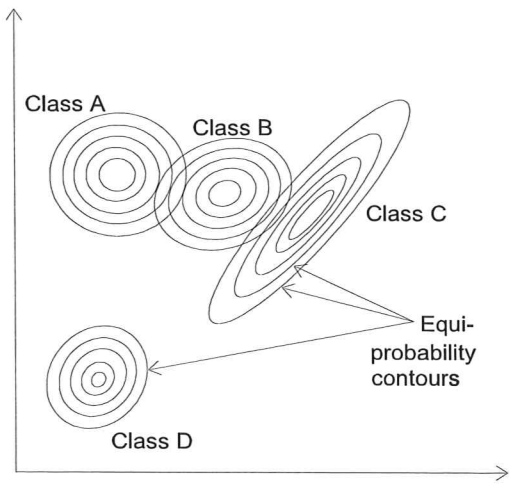

Figure 5. Equiprobability contours in a two dimensional data space as defined by the maximum likelihood classifier (modified from Lillesand and Kiefer, 1987).

Before the image data is classified the training data should be evaluated. The spectral classes must not overlap, but should describe as much as possible of the natural variation within each land-cover class. The training data set is assessed either statistically or graphically. The latter involves the display of histograms or box plots for data points included in the training areas for each land cover type. Therefore, the amount of overlap between classes may be easily detected. An analysis of variance approach can be used to determine whether or not there is a significant difference among class means. The F-test statistics (F) is a ratio of the summary measure of the variability among sample means, and the summary measure of the variability within the sample (Hawkes, 1993; Berenson *et al.* 1983). With an increasing variability among the sample means relative to the variability within the sample observations, the value of F will become large casting doubt on an assumption that the class means are the same. Therefore the vegetation indices may be ranked in ascending class separability.

In order to classify the different vegetation indices, a limit on all classes that spectrally overlap must be found. Assuming the pixels are normally distributed around the mean, this limit value (G) can easily be found (Eklundh and Pilesjö. 1987), see figure 6. The standard deviations for each class are represented by s1 and s2, and the mean value for the class by $\bar{x}1$ and $\bar{x}2$. The distance to G, in standard deviations from each class mean, are calculated from the formula:

$$\text{Distance to G} = \frac{|\bar{x}1 - \bar{x}2|}{(s1 + s2)}$$

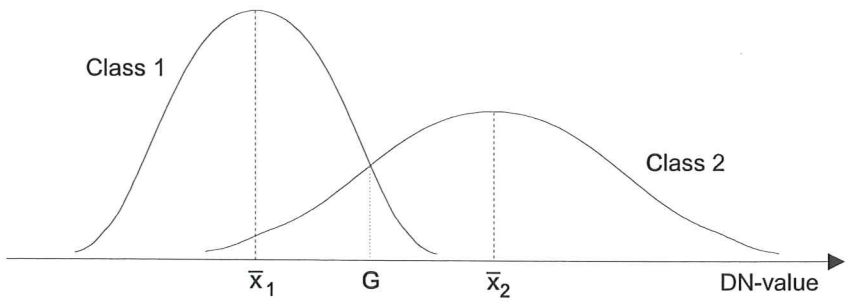

Figure 6. Schematic illustration to find the limit (G) between two normally distributed classes. At G the probabilities of a pixel belonging to class 1 and class 2 are equal (source: Eklundh and Pileslö, 1987).

2.8 POST CLASSIFICATION FILTERING

Classification of digital images can result in rather speckled images with unnaturally inhomogenous areas. A mode filter will clean up the images and produce more homogenous areas, but will also remove many linear and small features. The mode filter computes the most frequent occurring DN-value within the filter window surrounding each pixel. A 5 x 5 pixel mode filter window was chosen in this study to clean the classified images to visually resemble the generalisation of the desertification map.

2.9 ESTIMATING ACCURACY ON THE CLASSIFIED IMAGES

After having classified satellite image data it is necessary to evaluate the resemblance of the produced thematic map with the landscape it is supposed to describe. This is most often accomplished by comparing classified image pixels with ground truth data collected at the time of the image registration in the field (control points). In this study, where Landsat MSS data is used in order to map desertification degree areas in accordance with the Chinese classification system, a thematic map (Desertification map of Horqin Grassland 1:500.000) rather than field data is used to evaluate the accuracy of the classification results.

Several schemes for control point sampling and statistical accuracy evaluation has been suggested (Lillesand and Kiefer, 1987). Van Genderen *et al.* (1977; 1978) argued for a sample size of at least 20 per vegetation or land cover category for an interpretation accuracy of 80% and a minimum of 30 points for 90% accuracy at the 5% probability level. Hay (1979) and Congalton (1991) use a minimum of 50 samples for each category as a rule of thumb. Numerous recommendations on how to sample control points in the field or from any other source to be used as validation in the evaluation procedure are to be found, such as; random, systematic or stratified sampling. A good and up-to-date review on accuracy assessment of remote sensing data can be found in two articles by Congalton (1988; 1991).

The standard procedure for representing accuracy, recommended by Helldén (1980) and Congalton (1991), is in the form of an error matrix. An error matrix is a square array of numbers in rows and columns which express the number of sampled pixels assigned to a

particular class relative to the actual class as verified from the source of truth. The columns represent the classification result and the rows the reference data. Hereafter the error matrices can be used as the starting point for a number of descriptivė statistical techniques for the evaluation of accuracy. The simplest measure is the total accuracy which is computed by dividing the total correctly classified pixels (the sum of the major diagonal) by the total number of pixels in the error matrix. In a similar way the accuracy of each class can be computed. This, however, offers several different options; The correct classified pixels can be divided either by the total number of pixels in the corresponding column or row. In addition to this, a combination of the two will give a mean accuracy. The mean accuracy is the probability that a randomly chosen point of a specific class on the generated image has a correspondence of the same class and in the same position in the truth source and that a randomly chosen point in the truth source of the same class has a correspondence of the same class in the same position on the image. Helldén (1977) also introduced an indicator called areal difference to accompany the indicators of individual class accuracy. The areal difference describes how many per cent a specific class on the generated images has been over- or underestimated in relation to the sampled truth.

Most commonly the "producer's accuracy" also called "classification accuracy" is used. It is calculated by dividing the total number of correct pixels in a category by the total number of pixels of that category in the reference data. This measure indicate the probability that a point chosen at random from the truth source has a correspondence of the same class, at the same position, in the generated image. On the other hand, if the total number of correct pixels in a class is divided by the by the total number of pixels that were classified into that category, we produce the "user's accuracy" or "object accuracy". This measure denotes the probability that a pixel classified on the image actually represent that category in the truth source, rather than describing how much of the environment has a resemblance on the image. The statistical formulas used in the evaluation of the classification accuracy are presented in table **3**.

Table 3. Definition of the indicators of mapping accuracy (source: Helldén 1980)

N	=	total number of control points
A	=	the number of correctly mapped data for a specific class
ΣA	=	the total number of correctly mapped data (all classes included)
B	=	the number of sampled truth source data for a specific class
C	=	the number of map data for a specific class

Producer's accuracy, classification accuracy: (A / B) x 100, denotes the probability that a randomly chosen point of a specific class in the truth source has a correspondence of the same class in the same position on the map/image

User's accuracy, object accuracy: (A / C) x 100, denotes the probability that a randomly chosen point of a specific class on the map/image has a correspondence of the same class in the same position in the truth source.

Areal difference: ((C - B) / B) x 100, denotes with how many per cent a specific class on the map/image has been overestimated(+) or underestimated(-) in relation to the sampled truth source data for that particular class.

Mean accuracy: (2 x A / (B + C) x 100, denotes the probability that a randomly chosen point of a specific class on the map/image has a correspondence of the same class in the same position in the truth source *and* that a randomly chosen point in the truth source of the same class has a correspondence of the same class in the same position on the map/image.

Total accuracy: (ΣA / N) x 100, denotes the probability that a randomly chosen point on the map/image has a correspondence of the same class in the same position in the truth source *and* that a randomly chosen point in the truth source has a correspondence of the same class in the same position on the map/image.

---

3. METHODOLOGY

In effort to clarify the practical aspect of the theoretical background given in the previous section, the working procedure is stated step-by-step below.

- The satellite data is read to an EASI/PACE PCI database from magnetic CCT tapes.
- The satellite image bands are then checked for systematic errors such as line drops or striping.
- Ground control points for the geometric registration are identified on both the image and the desertification map. A geometric correction package within the image processing software, together with a digitizing tablet, are used to geometrically register the image to the desertification map via a polynomial function.
- Four different vegetation indices are computed, and MSS band 6 alone is used as a vegetation index as well.
- Principal component analysis is run on the raw satellite data, and the two first components are used as vegetation indices in the evaluation.
- A digitized version of the desertification map (digitised at the Institute of Remote Sensing Applications, Beijing) is imported to the image processing software. This will allow for easy training site selection and accuracy assessment.

- The polygon contours from the map are laid over the satellite image and training sites are chosen from areas in the center of polygons identified as any of the four desertification risk classes on the desertification map.
- Numerical data from the training sites of all vegetation indices are read and statistically and graphically evaluated.
- The DN-value width of classes in standard deviation from the mean value of the training data are decided upon, and thresholds between classes with spectral overlap are calculated to allow for classification of the vegetation indices.
- The vegetation indices are single band classified and the four original MSS bands are classified with the maximum likelihood algorithm.
- Each classified image is mode filtered to produce more homogenous areas that resembles the degree of generalisation on the desertification map.
- Control points are systematically sampled from the desertification map for accuracy evaluation of the classified images.
- Finally, error matrices are constructed for all classified vegetation index images, and accuracy indicators are calculated and evaluated.

3.1 PREPROCESSING

The satellite image data in this study was selected to coincide with the peak growing season and the compilation of the desertification map of the Horqin Sandy Land. The Landsat5 MSS image data from August 22nd, 1991 (path 121, row 30, approximate image centre, 121°E / 41°N) was bought from the Remote Sensing Technology Centre of Japan (RESTEC), where the information in table 4 was acquired. Earth-sun distance values were read from The Astronomical Almanac (1991). All image data analysis was conducted with the EASI/PACE PCI software (V 5.2 on UNIX station, V5.3 and V6.0 on PC platform)

Table 4. Bandwidths (nm), post-calibration dynamic ranges ($mW/cm^2/\mu m/sr$), DN maximum values, and mean solar exoatmospheric spectral irradiances ($mW/cm^2/\mu m$) for the Landsat 5 MSS-data used in this study (RESTEC pers. com.).

Platform	MSS Band	Band Width	Lmin	Lmax	Esun	DNmax
Landsat 5 RESTEC 910822	1	116.2	0.34	20.48	184.9 ± 0.2	127
	2	98.8	0.48	16.60	159.5 ± 0.3	127
	3	116.3	0.43	12.21	125.3 ± 0.1	127
	4	275.2	0.44	12.68	87.03 ± 0.7	127

The radiometric correction was performed by employing the equations provided by Markham and Barker (1986). Maximum and minimum at satellite reflectance for the four MSS bands were computed, and then uniformly rescaled to 8-bit data by multiplying with a gain of 417.1804 and subtracting by an offset of 6.006. When these calculations have been performed the actual image data was radiometrically corrected by a simple linear stretch. The 32-bit at satellite reflectance values for bands 2 and 4 were retained for calculation of NDVI and SAVI as recommended by Goward *et al.* (1991).

The image was geometrically corrected by registering it to the 1:500,000 scale desertification map via a second order polynomial transformation with a pixel estimate standard error of 4.2 pixels, and a line estimate standard error of 4.6 pixels. A total of 23 ground control points were used in the transformation. Reflectance values were interpolated using the nearest neighbour resampling method. The registration procedure reduced the pixel size to 64.8 meters in both x and y directions. A total of 6,045,298 pixels makes up a study area of 25,384 km^2.

3.2 IMAGE PROCESSING

The four vegetation indices; NDVI, RVI, DVI, and SAVI were computed from the at-satellite reflectance values (not rescaled for the NDVI and the SAVI). An adjustment factor of 0.5 was used to calculate the SAVI. The soil line slope in the NIR-red wavebands spectral plot was estimated to 1.0, and the index was thus unchanged by its multiplication constant.

The first two principal components of the raw image data were calculated, and the image data was rescaled to 8-bit data with data midpoint value of 127.5. The first component (PC1) was found to contain 88.4% of the variation, and the second component (PC2) 10.7%.

To check the interrelation between image channels, a correlation matrix was computed for the four original wavebands, and for the vegetation indices (Table 5). High inter-band relationship was found in the typically high correlated MSS bands. High correlation was also found between the vegetation indices, apart from MSS band 6 and the first principal

component (PC1), which were also used as estimators of vegetation cover. PC1, on the other hand, is highly correlated to the original wavebands.

Table 5.Correlation matrix for the original bands and the vegetation indices.

	MSS4	MSS5	MSS6	MSS7	DVI	RVI	PC1	NDVI
MSS5	0.983							
MSS6	0.823	0.821						
MSS7	0.654	0.641	0.938					
DVI	-0.849	-0.878	-0.465	-0.196				
RVI	-0.661	-0.709	-0.291	-0.036	0.884			
PC1	0.971	0.975	0.924	0.790	-0.754	-0.571		
NDVI	-0.674	-0.705	-0.207	0.069	0.944	0.907	-0.542	
SAVI	-0.678	-0.710	-0.206	0.080	0.957	0.903	-0.542	0.992

3.3 IMAGE CLASSIFICATION

The digitized desertification map was laid over the image to assist in training site selection. Eight sites distributed over the entire image for each of the four desired classes were identified. These sites were chosen such that they were in the centre of desertification class polygons on the 1991 desertification map and at the same time coinciding with the same class on the older desertification map (early 1980's). This procedure was used to ensure that training sites were chosen, from a vegetation status point of view, relatively stable areas.

An iterative single band classification approach of the vegetation indices was used to decide upon the DN value width of each class. Ninety-five per cent (± 1.96 standard deviations from the mean) of the sampled training data for each class was used to classify the images. Where spectral overlap between classes was found, the limit was calculated according to the equation provided by Eklundh and Pilesjö, (1987). Table 5 (section 4) shows the DN range for each class in the six vegetation indices.

DN values from each desertification class, for the six vegetation indices, were extracted for descriptive statistic evaluation. Boxplots were made for visual interpretation of spectral overlap, and F-test statistics gives a pointer to the separability between classes in the vegetation indices.

3.4 ACCURACY ASSESSMENT

A systematic sampling was chosen to draw control points from the thematic desertification risk map of Horqin sandy land (1991). A total of 432 samples separated by 120 pixels in both x and y directions were taken from the classification results. Control points not falling within the area defined as the alluvial plain of Xiliao River, together with the unclassified pixels were excluded from the analysis, as the objective was only to study the plain affected by wind erosion. The result of the sampling was put into error matrices. User's, producer's, mean, and total accuracy was chosen to be used as accuracy estimates together with the areal difference measure.

4. RESULTS

The results of the separability analysis and the class limits calculations used for the vegetation indices images are presented in boxplots (fig. 8) and in Table 6. The overlap between classes in the different vegetation indices vary quite a bit. The training statistics for the second principal component image showed the greatest overlap, and will not allow for acceptable separation between classes, and was therefore excluded from the analysis. Based on the F-test statistics, the indices show separability between classes in the following ascending order: PC1, Band 6, DVI, NDVI, SAVI, RVI.

Table 6. Descriptive statistics, and F-test statistics from the analysis of variance for the four desertification degree classes in all vegetation indices. N is the total number of training data pixels for each class.

Band 6
F-test = 3463

Class	N	Mean	Median	StDev	Min	Max	-1.96*	+1.96*
Latent	309	119.5	116	12.5	91	157	95	*128*
Slight	456	133.9	133	7.8	113	158	*129*	*139*
Moderate	299	159.3	160	9.7	138	181	*140*	*175*
Severe	319	192.2	194	9.5	166	214	*176*	211

DVI
F-test = 2136

Class	N	Mean	Median	StDev	Min	Max	-1.96*	+1.96*
Latent	309	145.3	145	13.8	112	193	*133*	172
Slight	456	124.1	126	9.1	92	147	*118*	*132*
Moderate	299	109.1	108	10.2	86	139	93	*117*
Severe	319	84.5	85	4.9	72	99	75	92

RVI

F-test = 835

Class	N	Mean	Median	StDev	Min	Max	-1.96*	+1.96*
Latent	309	30.4	29	7.5	18	59	*24*	45
Slight	456	21.2	21	2.3	14	29	*19*	*23*
Moderate	299	18.4	18	1.8	15	25	*17*	*18*
Severe	319	15.9	16	0.6	14	18	15	*16*

PC1

F-test = 4627

Class	N	Mean	Median	StDev	Min	Max	-1.96*	+1.96*
Latent	309	107.2	104	10.9	85	137	86	*118*
Slight	456	125.8	125	7.6	110	149	*119*	*136*
Moderate	299	151.4	152	10.3	130	172	*137*	*171*
Severe	319	188.0	190	8.8	164	206	*172*	205

NDVI

F-test = 1026

Class	N	Mean	Median	StDev	Min	Max	-1.96*	+1.96*
Latent	309	155.3	155	10.0	135	186	*147*	175
Slight	456	141.3	142	5.4	119	156	*139*	*146*
Moderate	299	135.8	136	4.6	126	151	*132*	*138*
Severe	319	129.3	129	2.0	121	135	125	*131*

SAVI

F-test = 878

Class	N	Mean	Median	StDev	Min	Max	-1.96*	+1.96*
Latent	309	144.6	144	6.2	132	167	*140*	157
Slight	456	136.8	137	3.7	121	145	*135*	*139*
Moderate	299	133.4	133	3.5	125	145	*131*	*134*
Severe	319	128.4	128	1.8	122	134	125	*130*

** Values given as ± 1.96 standard deviations from the mean if no overlap between classes were found. In case of overlap the values are in italic.*

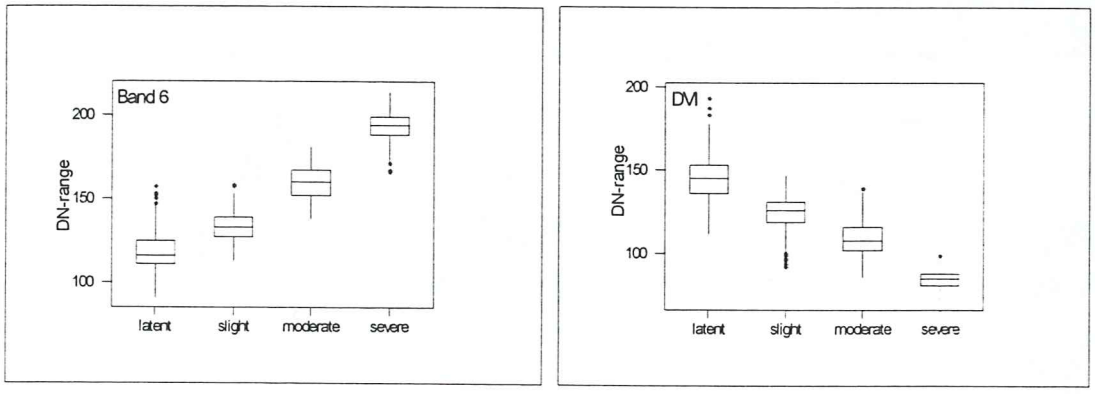

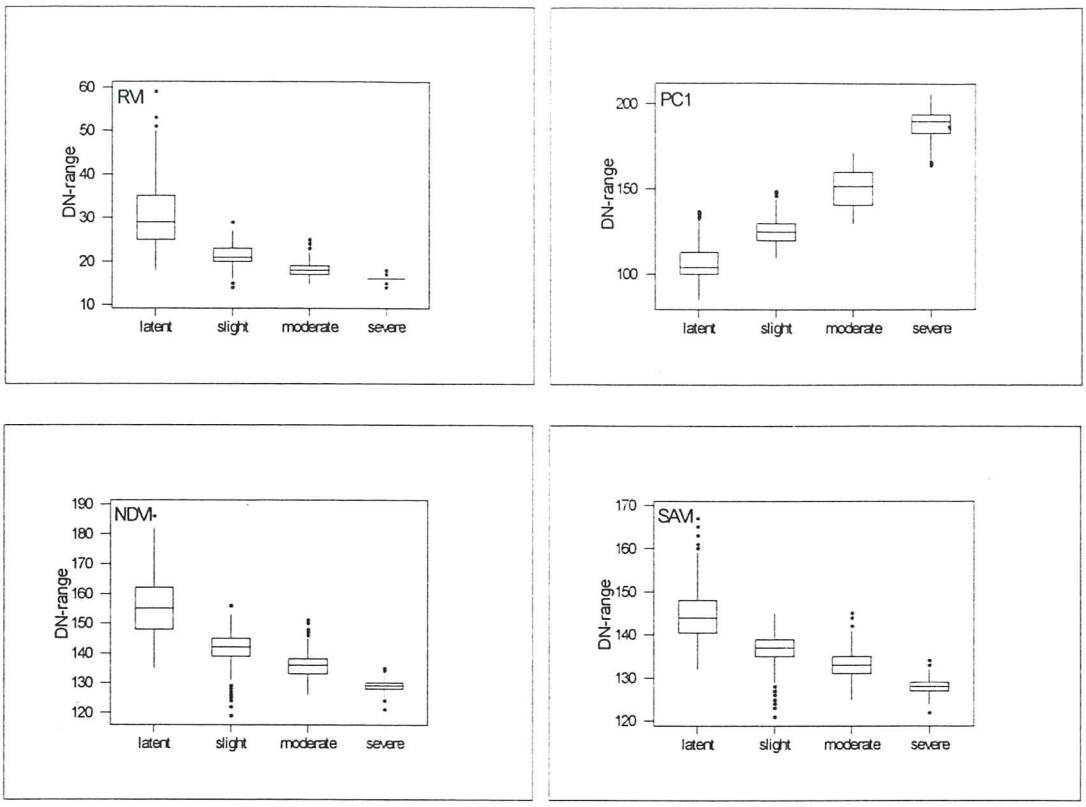

Figure 8. Boxplots showing the separability the four desertification classes in the six vegetation indices. The boxes describe the interquartile range Q1 to Q3 (i.e. 75% of the data within each class). The lines that extend from the top and bottom of the boxes, are defined as Q1 - 1.5 (Q3 - Q1) for the lower limit, and Q1 + 1.5 (Q3 - Q1) for the upper limit. Outliers are points outside the lower and upper limits, plotted with asterisks (*).

4.1 THE CLASSIFICATION

The maximum likelihood classification (of the four original wave bands) and the classification of the vegetation indices resulted in four desertification risk classes: latent, slight, moderate, severe, and no-identified pixels that seems to include water bodies, marshlands, mountainous areas, urban areas, and some cultivated land. The areal extent of each class are rather different among the different vegetation indices. The area of latent risk makes up 31-43% of the total area, slight risk 22-31%, moderate risk 13-33%, severe risk 6-12%, and unclassified 1-10%.

A 5 x 5 pixels mode filter was used to clear the images and produce more homogenous areas of the five classes. Filtering the images had quite a small influence of the areal extent of classes within the images. No more than a 2% change in area was found when comparing filtered with non-filtered classified images.

Figure 9 shows subscenes and reference data, approximately 53 by 39 kilometers in size, of the classified and filtered vegetation indices images. The reference data is a taken from the digitised desertification map. Polygon vectors from the reference data is overlaid the vegetation indices for comparison.

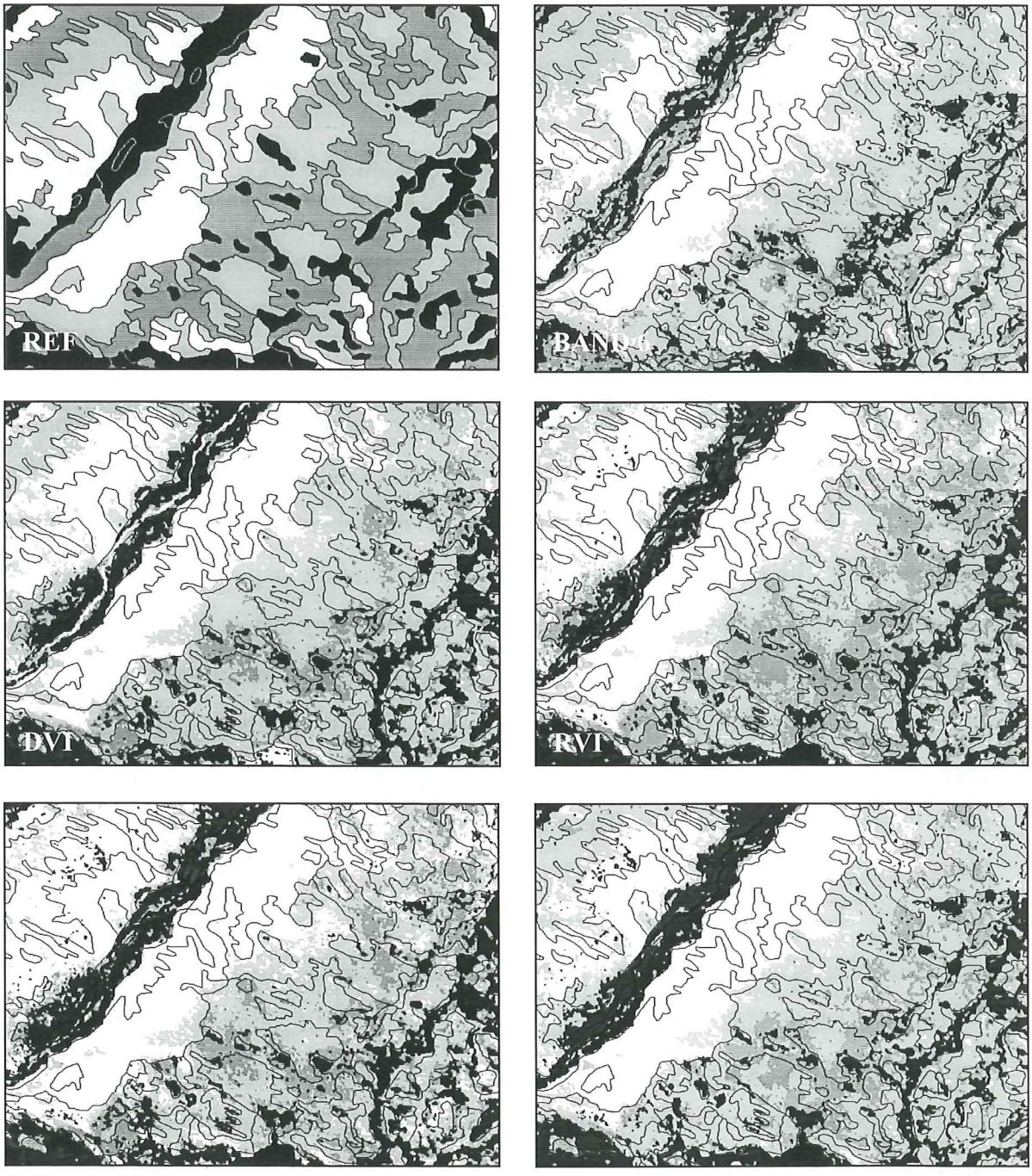

PC1 NDVI

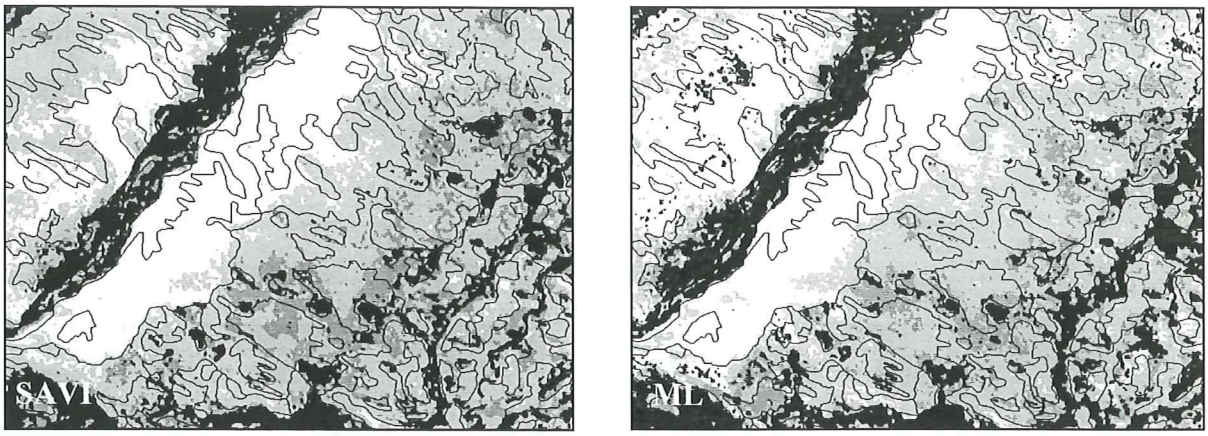

Figure 9. Selected subscenes for visualisation of the filtered classification results, and the reference data. White through dark gray depicts severe, moderate, slight, and latent desertification degree. Black is unclassified pixels .

4.2 ACCURACY ASSESSMENT

Table 7 shows fourteen error matrices for the classified images, including both raw classified image data and the filtered image data. Rows represent the control data, and columns the classified image data. Total accuracy was calculated in two ways. One where only the four desertification classes are included, an one where areas classified as latent but coinciding with areas marked as farmland on the reference map were included as belonging to the latent desertification class. The total accuracy differs from 39.6% to 54.8%, with most results at about 48%. Including the farmland areas in the latent desertification class improved the result with up to 7.4% (DVI). Filtering the images did improve accuracy for all classification results, except for the DVI with farmlands included in the latent desertification class. The improvement for the total accuracy was however low, no more than 4.5%.

Individual class accuracy estimates, on the other hand, were greatly affected by the mode filtering procedure. This is most striking for the severe desertification class which in most cases increased user's accuracy by about 12%, and as much as 15.4% for PC1. User's accuracy above 70% for the severe class was found for all classification results, apart from NDVI and SAVI. The improvement of user's accuracy for the severe class was mostly accounted for by the reduction of misclassified pixels in the latent, slight, and moderate

categories, and only to a small extent by the reduction of misclassified pixels to the moderate and slight classs. The producer's accuracy measurements did not show the great inter class differences. This is reflected in the difference between user's and producer's accuracy for the severe class, which is greatly underestimated (se areal difference) with all vegetation indices.

The moderate and slight desertification classes showed very low accuracy in the range of 19.6% (RVI) to 46.7% (SAVI). Latent desertification accuracy was about 60% for all classification results. No vegetation index accuracy stands out as particularly good in comparison to the others. It is, however, worth noticing that both the NDVI and SAVI has much lower inter-class user's accuracy differences than any of the other vegetation indices. NDVI and SAVI also show the least areal difference, about ±12% for NDVI and ±5% for SAVI.

Tendencies for misclassification becomes clear when studying the error matrices in detail. The latent desertification class is misclassified tothe slight category, and vise versa. The moderate desertification class, however, is not confused by its neighbouring classes, but to an equal extent misclassified as slight and latent. The severe desertification class is mostly misclassified as moderate.

Table 7. Error matrices for all vegetation indices, both the raw classified data and the mode filtered, classified data. Rows represents the control data, and columns the actual classified data. Farmland (from the reference data) is counted as belonging to the latent class in the classified data. Total does include only the four desertification degree classes. Indicators of accuracy are given in per cent: UA = user's accuracy, PA = producer's accuracu, MA = mean accuracy, AD = areal difference, and TA = total accuracy.

Band6

	latent	slight	moderate	severe	unclass.	Total	UA	PA	MA	AD	TA
latent	56	36	39	1	2	133	56.6	42.1	48.3	-34.3	
slight	32	26	30	3	0	91	32.9	28.6	30.6	-13.2	
moderate	9	13	21	6	1	50	19.6	42.0	26.8	114	
severe	2	4	17	24	0	47	70.6	51.1	59.3	-27.7	
unclass.	22	23	23	0	6	74					
farmland	17	14	6	0	0	37					
Total incl. farmland	116	93	113	34		358					40.2
Total	99	79	107	34	9	321					39.6

Band6 filtered

	latent	slight	moderate	severe	unclass.	Total	UA	PA	MA	AD	TA
latent	60	29	42	0	2	133	58.3	45.1	50.8	-22.6	
slight	35	25	31	0	0	91	38.5	27.5	64.1	-28.6	
moderate	7	9	29	4	1	50	23.2	58.0	33.1	150	
severe	1	2	24	19	1	47	82.6	40.4	54.3	-51.1	
unclass.	21	22	26	0	5	74					
farmland	17	14	6	0	0	37					
Total incl. farmland	120	79	131	23	9	358					41.9
Total	103	65	125	23	9	321					41.4

DVI

	latent	slight	moderate	severe	unclass.	Total	UA	PA	MA	AD	TA
latent	72	34	17	2	8	133	60.0	54.1	56.9	-9.8	
slight	33	36	18	2	2	91	40.4	39.6	40.0	-2.2	
moderate	13	10	23	4	0	50	31.5	46.0	37.4	46.0	
severe	2	9	15	21	0	47	72.4	44.7	55.3	-38.3	
unclass.	41	19	8	2	4	74					
farmland	24	3	1	1	8	37					
Total incl. farmland	144	92	74	30	20	358					54.8
Total	120	89	73	29	22	321					47.4

DVI filtered

	latent	slight	moderate	severe	unclass.	Total	UA	PA	MA	AD	TA
latent	74	33	15	1	10	133	59.7	55.6	57.6	-6.8	
slight	35	39	16	0	1	91	44.8	42.9	43.8	-4.4	
moderate	10	12	25	3	0	50	34.2	50.0	40.7	46.0	
severe	5	3	17	22	0	47	84.6	46.8	60.3	-44.7	
unclass.	42	16	9	2	5	74					
farmland	22	2	2	0	11	37					
Total incl. farmland	146	89	75	26	22	358					50.8
Total	124	87	73	26	11	321					49.8

RVI

	latent	slight	moderate	severe	unclass.	Total	UA	PA	MA	AD	TA
latent	65	44	8	4	12	133	58.6	48.9	53.3	-16.5	
slight	31	45	11	2	2	91	38.8	49.5	43.5	27.5	
moderate	13	15	16	6	0	50	34.0	32.0	33.0	-6.0	
severe	2	12	12	20	1	47	62.5	42.6	50.6	-31.9	
unclass.	40	21	1	4	8	74					
farmland	22	4	0	0	11	37					
Total incl. farmland	133	120	47	32	26	358					46.9
Total	111	116	47	32	15	321					45.5

RVI filtered

	latent	slight	moderate	severe	unclass.	Total	UA	PA	MA	AD	TA
latent	69	43	7	2	12	133	60.0	51.9	55.6	-13.5	
slight	32	44	11	1	3	91	38.3	48.4	42.7	26.4	
moderate	11	19	15	4	1	50	34.1	31.9	31.9	-12.0	
severe	3	9	12	23	0	47	76.7	48.9	59.7	-36.2	
unclass.	39	22	0	3	10	74					
farmland	21	3	1	0	12	37					
Total incl. farmland	136	118	45	30	28	358					48.0
Total	115	115	44	30	16	321					47.0

PC1

	latent	slight	moderate	severe	unclass.	Total	UA	PA	MA	AD	TA
latent	63	48	20	1	1	133	53.8	47.4	50.4	-12.0	
slight	40	29	21	1	0	91	29.3	31.9	30.5	8.8	
moderate	13	15	17	5	0	50	22.7	34.0	27.2	50.0	
severe	1	7	17	22	0	47	75.9	46.8	57.9	-38.3	
unclass.	31	34	6	0	3	74					
farmland	29	6	2	0	0	37					
Total incl. farmland	146	105	77	29	1	358					44.7
Total	117	99	75	29	1	321					40.8

PC1 filtered

	latent	slight	moderate	severe	unclass.	Total	UA	PA	MA	AD	TA
latent	67	44	22	0	0	133	60.9	50.4	55.1	-17.3	
slight	34	35	22	0	0	91	35.7	38.5	37.0	7.7	
moderate	7	15	25	2	1	50	28.1	50.0	36.0	78.0	
severe	2	4	20	21	0	47	91.3	44.7	60.0	-51.1	
unclass.	32	33	6	0	3	74					
farmland	28	9	0	0	0	37					
Total incl. farmland	138	107	89	23	1	358					49.2
Total	110	98	89	23	1	321					46.1

NDVI

	latent	slight	moderate	severe	unclass.	Total	UA	PA	MA	AD	TA
latent	69	33	11	7	13	133	59.5	51.9	55.4	12.8	
slight	31	38	13	7	2	91	43.7	41.8	42.7	-4.4	
moderate	13	10	20	6	1	50	33.9	40.0	36.7	18.0	
severe	3	6	15	20	3	47	50.0	42.6	46.0	-14.9	
unclass.	42	16	4	2	10	74					
farmland	23	3	1	0	10	37					
Total incl. farmland	139	90	60	40	29	358					47.5
Total	116	87	59	40	19	321					45.8

NDVI filtered

	latent	slight	moderate	severe	unclass.	Total	UA	PA	MA	AD	TA
latent	72	32	12	5	12	133	60.0	54.1	56.9	-9.8	
slight	33	41	12	2	3	91	45.6	45.1	45.3	-1.1	
moderate	10	13	19	5	3	50	44.2	38.0	40.9	-14.0	
severe	5	4	15	22	1	47	64.7	46.8	54.3	-27.7	
unclass.	41	16	4	3	10	74					
farmland	22	1	1	0	13	37					
Total incl. farmland	142	91	44	34		358					49.2
Total	120	90	43	34	19	321					48.0

SAVI

	latent	slight	moderate	severe	unclass.	Total	UA	PA	MA	AD	TA
latent	70	38	6	9	10	133	57.9	52.6	55.1	-9.0	
slight	35	34	13	7	2	91	37.0	37.4	37.2	1.1	
moderate	11	14	18	6	1	50	37.5	36.0	36.7	-4.0	
severe	5	6	11	22	3	47	50.5	46.8	48.4	-6.4	
unclass.	43	15	3	0	9	74					
farmland	24	4	0	0	9	37					
Total incl. farmland	145	96	48	44	25	358					46.9
Total	121	92	48	44	16	321					44.9

SAVI filtered

	latent	slight	moderate	severe	unclass.	Total	UA	PA	MA	AD	TA
latent	73	32	10	6	12	133	59.8	54.9	57.3	-8.3	
slight	32	42	12	2	3	91	46.7	46.2	46.4	-1.1	
moderate	12	11	15	10	2	50	31.9	30.0	30.9	-6.0	
severe	5	5	10	26	1	47	59.1	55.3	57.1	-6.4	
unclass.	44	12	4	4	10	74					
farmland	23	2	0	0	12	37					
Total incl. farmland	145	92	47	44	30	358					50.0
Total	122	90	47	44	18	321					48.6

ML

	latent	slight	moderate	severe	unclass.	Total	UA	PA	MA	AD	TA
latent	64	44	17	2	6	133	61.0	48.1	53.8	-21.1	
slight	28	40	19	2	2	91	38.8	44.0	41.2	13.2	
moderate	11	14	18	4	3	50	25.7	36.0	30.0	40.0	
severe	2	5	16	22	2	47	73.3	46.8	57.1	-36.2	
unclass.	39	22	5	1	7	74					
farmland	31	4	1	0	1	37					
Total incl. farmland	136	107	71	30	14	358					48.9
Total	105	103	70	30	13	321					44.9

ML filtered

	latent	slight	moderate	severe	unclass.	Total	UA	PA	MA	AD	TA
latent	72	35	22	0	4	133	61.0	54	57.4	-11.3	
slight	33	38	19	0	1	91	44.2	41.8	42.9	-5.5	
moderate	11	11	21	4	3	50	25.9	42.0	32.1	62.0	
severe	2	2	19	21	3	47	84.0	44.7	58.3	-46.8	
unclass.	42	17	7	1	7	74					
farmland	34	3	0	0	0	37					
Total incl. farmland	152	89	81	25	11	358					52.0
Total	118	86	81	25	11	321					47.4

5. DISCUSSION

5.1 GEOMETRIC PRECISION

The image to map registration resulted in an error of as much as 300 meters in the y-direction. This is not an acceptable error in many image analysis applications. The scale of the map (1:500.000) to which the image was registered is the source of the large errors. Ground control points such as road and railroad intersections were carefully chosen, but the degree of generalisation in the map made precision at MSS data pixel level virtually impossible. Roads, 0.7 mm in width on the map represents 350 meters in reality. The result was not considered crucial for the study, and no extra effort was put into increasing the precision. If images from other time periods were to be used in a change study it would be preferable to carry out an image to image registration rather than image to map.

5.2 CLASSIFICATION TRAINING DATA

In this study the desertification map of the Horqin grassland (1991) was used as the source both for training data, for the classifications, and as reference data for the accuracy assessment. This approach might be argued as dubious, but was considered appropriate since different samples were used for training data and accuracy evaluation. The map should be used as reference data for estimating accuracy as the aim was to see whether or not it was possible to produce a result similar to the map. The method employed assumes that the classes found on the map can be estimated solely from the vegetation cover over a specific area, and that satellite image derived vegetation indices can be used as indicators. One should bear in mind that the collected training data were not only based on vegetation cover but also on biomass change, and deflation and deposition. Undoubtedly, the most rigid way to select training areas would be from field measurements on green vegetation cover. And, if continuous monitoring methods like the one presented here were to be implemented, several of the research field stations in the area could be used for supplying training data from well defined locations that are vegetationally stable from one year to another.

5.3 ACCURACY EVALUATION

A total accuracy measure of about 50% does not show any convincing results for any of the classified vegetation indices. The total accuracy of 54.8% for the DVI; with farmland included in the latent desertification class was the best result. Farmlands were included in the latent class in the accuracy assessment because it coincides with latent desertified areas on the map. The slight increase in total accuracy by mode filtering the images can probably be explained by the confusion between the latent, slight, and moderate classes. Bare patches within these classes will be classified as severe, but will disappear after the image is mode filtered to produce more homogenous areas. This is also the explanation for the great increase of user's accuracy of the severe class after applying the mode filter.

The severe desertification class is characterised by semi-fixed and drifting sand dunes, and a vegetation cover of less than 10%. But during the rainy season, interdune depressions become waterlogged and vegetation can flourish for a short while. During this period misclassification of pixels that describe dense vegetation within bare sand dune areas may result. This problem was however successfully overcome with the application of a mode filter.

The moderate desertification class showes the overall lowest user's accuracy. It is to a large degree confused with both the latent and the slight class. This can be explained by the vegetation characteristics of the areas classified as moderate according to the Chinese classification system. Annual plants contribute up to 70% of the fresh biomass, primarily occurring in July and August. These areas will therefore, during the peak growing season, easily be confused with the vegetationally more dense slight and moderate classes. It could thus be argued that images registered at another time should be used. Without trying the same classification approach on images from earlier or later in the growing season, it is impossible to render which could perform better. One should, however, stick to the growing season. Otherwise, due to the low amount of perennial vegetation, the moderately desertified land would probably be confused with more severely degraded land.

There is no clear evidence to the low accuracy of the slight class. It is however clear that it is greatly confused with the latent class. Annual plants might again be the culprit. As the

image was registered at the peak growing season, the possibility exists that the vegetation characteristics of the latent and slight classes even out, due to the blooming of annual plants.

The maximum likelihood classification showed very similar results to the classification of the vegetation indices and the first principal component. This points to the vegetation being the contributor to the main variation of reflectance values inherent in the original image data.

6. CONCLUSION

A straight forward classification approach to continuous monitoring of land degradation severity in the Horqin Sandy Land has been put forth, but the study did not show any convincing results. The vegetation indices used for green cover estimation did not give large differences when classifying the images (*c.f.* Perry and Lautenschlager, 1984). These classifications also showed equal results with the first principal component, and the maximum likelihood classification. No single classification proved to be superior to the others.

The results did, however, give hints to what could be done to improve the remote sensing mapping. Training areas, with known vegetation cover, should preferably be chosen from the field. Choosing images registered at the beginning of the growing season might also improve the result, as the peak of annual vegetation could lead to an evening out of the desertification degree classes as observed from a vegetation status standpoint. Also, Landsat TM data derived vegetation indices may perform better. Elvidge and Chen (1995) compared vegetation indices produced from different satellite sensors and found a 10% increase in estimating green vegetation cover with TM data as compared to MSS data.

7. SUMMARY

The Chinese steppe ecosystem has been subject to destructive impact from man for at least the two last thousand years. In recent times the situation has worsened, and a national programme for monitoring of arid, semi-arid and sub-humid areas has been implemented by the Chinese academy of science. Under this programme several regions have been thematically mapped in a scale of 1:500,000. Areas have been classified into four degrees of desertification (latent, slight, moderate, and severe) on the basis of vegetation cover, biomass change, deflation, and deposition. In this study it is hypothesised that the Chines classification scheme can be reproduced only by studying the green vegetation cover as estimated with Landsat MSS data derived vegetation indices. A efficient way to classify the regions by using solely satellite data would enable monitoring on a yearly basis of the areas, rather than on a decadal basis which is now the case.

A straight forward procedure for classifying the vegetation indices is put forth. The ratio-, difference-, normalized-, and soil adjusted vegetation indices are tested together with MSS band 6, the first principal component, and the maximum likelihood algorithm in classifying the images in accordance with the Chinese classification system. The results are evaluated for accuracy using The Map of Desertification in Horqin Grassland, 1:500,000 (1991), Lanzhou Institute of Desert Research, Chinese Academy of Science, as reference data. The different vegetation indices show very similar classification accuracy results, and no single index stand out as superior to the others. Total accuracy at about 48% is found for most indices. Individual class accuracy estimates are highly variable, with mean accuracy in the range of 26.8% to 64.1%.

The low accuracy can probably be related to the fact that the image was registered at the peak growing season when annual vegetation makes distinguishing of different stages of land degradation on the basis of green vegetation cover virtually impossible.

It is concluded that if monitoring by satellite remote sensing are to be implemented as a complement to the currents mapping schemes, refinements to the classification procedure presented here has to be done.

REFERENCES

LITTERATURE

Ahlcrona, E., 1988, *The Impact on Land transformation in Central Sudan, Applications of Remote Sensing*, Meddelanden från Lunds Universitets Geografiska Institutioner, avhandlingar 103, 140p.

Ashley, M.D. and Rea, J.,1975. Seasonal vegetation differences from ERTS imagery. *Photogrammetric Engineering and Remote Sensing,* 41, 713-719

Asras, G., Fuchs, M., Kanemasu, E.T. and Hatfield J.L., 1984. Estimating absorbed photosynthetica radiation and leaf area index from spectral reflectance in wheat. *Agronomic Journal*, 76, 300-306.

Astronomical Almanac, 1991. *Nautical Almanac Office*, United States Naval Observatory, U.S. Government Printing Office, Washington.

Baret, F., Guyot, G. and Major, D.J., 1989. TSAVI: a vegetation index which minimizes soil brightness effects on LAI and APAR estimation, in *Proceedings of the 12th Canadian Symposium on Remote Sensing*, IGARRS'90, Vancouver, BC, Canada, 10-14 July, Vol. 3, 1355-1358.

Berenson, M.L., Levine, D.M. and Goldstein, M., 1983. *Intermediate statistical methods and applications, A computer package approach.* Prentice-Hall, Inc., Engelwood Cliffs, 579pp.

Bernstein, R. 1983. Image geometry and rectification, Chapter 21 in *The Manual of Remote Sensing,* R.N. Colwell, Ed. Falls Church, Va. American Society of Photogrammetry and Remote Sensing, Vol 1, pp 875-881.

Byrne, E.F., Crapper, P.F. and Mayo, K.K., 1980. Monitoring Land-Cover Change by Principal Components Analysis af Multitemporal Landsat Data. *Remote Sensing of Environment,* 10, 175-184.

Congalton R.G., 1988. A comparison of sampling schemes used in generating error matrices for assessing the accuracy of maps generated from remotely sensed data. *Photogrammetric Engineering and Remote Sensing,* 49, 1671-1678.

Congalton, R.G., 1991. A Review of Assessing the Accuracy of Classifications of Remotely Sensed Data. *Remote Sensing of Environment,* 37, 35-46.

Colwell, J.E.,1974. Vegetation canpoy reflectance. *Remote Sensing of Environment,* 3, 175-183.

Dregne, H.E., 1983. *Desertification of Arid Lands*, Harwood Academic Publishers, 242p.

Eklundh, L. and Pilesjö, P., 1987. Autmatisk skadeklassning av lövträd i stadsbebygelse med hjälp av digitaliserade IR-färgflygbilder. *Svensk Geografisk 63,* 228-242.

Elvidge, C.D. and Lyon, R.J.P., 1985. Influence of rock-soil spectral variation on the assessment of green biomass, *Remote Sensing of Environment*, 17, 265-269.

Elvidge, C.D. and Chen, Z., 1995. Comparison of Broad-Band and Narrow-Band Red and Near-Infrared Vegetation Indices, *Remote Sensing of Environment*, 54, 38-48.

Goward, N.S., Markham, B., Dye, D.G., Dulaney, W. and Yang, J., 1991. Normalized Difference Vegetation Index Measurements from the Advanced Very High Resolution Radiometer. *Remote Sensing of Environment*, 35, 257-277.

Graetz, R.D. and Gentle, M.R., 1982. The relationship between reflectance in the Landsat wavebands and the composition of an Australian semi-arid shrub range-land. *Photogrammetric Engineering and Remote Sensing,* 48, 1721-1730.

Hatfield, J.L., Kanemasu, E.T., Asrara, G., Jackson, R.D., Pinter, P.J., Reginato, R.J., and Idso, S.B., 1985. Leaf-area estimates from spectral measurements over various planting dates of wheat. *International Journal of Remote Sensing,* 6, 167-175.

Hawkes, J.S., 1993. *Discovering Statistics*. Quant Publishing, Charleston, S.C.

Hay, A.M., 1979. Sampling designs to test land-use map accuracy. *Photogrammetric Engineering and Remote Sensing,* 45, 529-533.

Helldén, U., 1977. Landsat data for environmental applications: Land-use mapping in the municipality of Linköping. *Statens Naturvårdsverk, SNV PM 892,* 48p.

Hellden, U., 1980. A test of Landsat-2 imagery and digital data for thematic mapping, illustrated by an environmental study in the northern Kenya. *Rapporter och Notiser* 44, Department of Physical Geography, Lund university.

Helldén, U., 1984. Drought Impact Monitoring, A Remote Sensing Study of Desertification in Kordofan, Sudan. *Rapporter och Notiser* 61, Department of Physical Geography, Lund university.

Holben, B.N., Tucker, C.J. and Fan, C.J., 1980. Spectral Assessment of Soybean Leaf Area and Leaf Biomass. *Photogrammetric Engineering and Remote Sensing,* 46, 651-656.

Huete, A.R., Post, D.F. and Jackson, R.D., 1984. Soil spectral effects on 4-space vegetation discrimination. *Remote Sensing of Environment*, 15, 155-165.

Huete, A.R., Jackson, R.D. and Post, D.F., 1985. Spectral response of a plant canopy with different soil backgrounds. *Remote Sensing of Environment*. 17, 155-165.

Huete, A.R. and Jackson, R.D. 1987. The suitability of spectral indices for evaluating vegetation characteristics on arid range-lands. *Remote Sensing of Environment*. 23, 213-232.

Huete, A.R., 1988. A Soil-Adjusted Vegetation Index (SAVI). *Remote Sensing of Environment,* 25, 295-309.

Huete, A.R., (1989). Soil influences in remotely sensed vegetation-canopy spectra, in Asrar, G., (ed.), *Theory and Applications of Optical Remote Sensing*. Wiley & sons, New York, 734p.

Ingbritsen, S.E. and Lyon, R.J.P., 1985. Principal Components Analysis of Multitemporal Image Pairs. *International Journal of Remote Sensing,* 6, 687-696.

Jensen, J.R., 1986. *Introductory Digital Image Processing, A Remote Sensing perspective.* Prentice-Hall, Engelwood Cliffs, New Jersey, 379p.

Jordan, C.F., 1969. Derivation of leaf area index from quality light on the forest floor. *Ecology*. 50, 663-666.

Kauth , R.J. and Thomas, G.S., 1976. The Tassled Cap - a graphical description of the spectral - temporal development of agricultural crops as seen by Landsat, in *Proceedings of the Symposium on Machine Processing of remotely Sensed Data,* Purdue University, West Lafayette, IN, 41-51.

Lillesand, T.M. and Kiefer, R.W., 1987. *Remote sensing and image interpretation.* John Wiley & sons, New York, 721p.

Markham, B.L. and Barker, J.L., 1986. Landsat MSS and TM post-calibration dynamic ranges. Exoatmospheric reflectance and at-satellite temperatures. EOSAT. *Landsat Technical Notes,* No. 1.

Mei, A.X. 1985. A study of grassland utilization conditions in the eastern parts of Inner Mongolia by analyzing Landsat MSS imagery, pp 723-724. In *Proceedings of the XV International grassland Cong,* Kyoto, Japan.

Misra, P.N. and Wheeler, S.G., 1977. Landsat data from agricultural sites - Crop signature analysis, *Proceedings of the 11th International Symposium on Remote Sensing of the Environment, ERIM.*

Nelson, R.F., 1985. Reducing Landsat MSS scene variability. *Photogrammetric Engineering and Remote Sensing*. 51, 35-48.

Olsson, L., 1988. Approached to monitoring renewable resources using remote sensing and geographical information system, pp 1041-1050, In *Proceedings of the seventh international symposium on remote sensing for resources development and environmental management, ISPRS commission VII / Enschede.*

Otterman, J. and Robinove, C.J., 1983. Landsat monitoring of desert vegetation growth, 1972-1979 using a plant shadowing model. *Advances in Space Research,* 2, 45-50.

Perry, C.R. and Lautenschlager, L.F., 1984. Functional Equivalence of Spectral Vegetation Indices. *Remote Sensing of Environment,* 14, 169-182.

Printer, P.J., Jackson, R.D., Ezra, C.E. and Gausman, H.W., 1985. Sun-angle and canopy-architecture effects on the spectral reflectance of six wheat cultivars. *International Journal of Remote Sensing,* 6, 1813-1825.

Richards, J.A., 1993. *Remote Sensing Digital Image Analysis, An Introduction.* Springer-Verlag, Berlin, 340p.

Richardson, A.J. and Wiegand, C.L., 1977. Distinguishing vegetation from soil background. *Photogrammetric Engineering and Remote Sensing*. 43, 1541-1552.

Robinove, C.J., Chavez, P.S., Ghering, D. and Holmgren, R., 1981. Arid land monitoring using Landsat albedo difference images. *Remote Sensing of Environment*, 11, 133-156.

Robinove, C.J., 1982. computation with physical values from Landsat digital data. *Photogrammetric Enginering and Remote Sensing,* 48, 781-784.

Rouse, J.W., Haas, R.H., Schell, J.A. and Deering, D.W., 1973. Monitoring vegetation systems in the great plains with ERTS, in *Third ERTS Symposium,* NASA SP-351, NASA, Washington, DC, Vol. 1, pp. 309-317.

Sellers, P.J., 1989. Vegetation canopy spectral reflectance and biophysical processes. In *Theory and Applications of Optical Remote Sensing,* edited by G. Asrar, New York: John Wiley, pp. 297-335.

Sheeny, D. P., 1992.A Perspective on Desertification of Grazing land Ecosystems in North China, *Ambio*, 21, No 4.

Swain, P.H. and Davies, S.M. (eds), 1978. Remote Sensing: The Quantitative Approach, N.Y. McGraw-Hill. 396p.

Tucker, C.J., 1979. Red and photographic infrared linear combinations for monitoring vegetation. *Remote Sensing of Environment,* 8, 127-150.

United Nations, 1977. *Desertification: Its Causes and Consequences.* Oxford, Pergammon Press.

United Nations Environmental Programme (UNEP), 1984. *General Assessment of Progress in the Implementation of the United Nations Plan of Action to Combat Desertification.* UNEP/GCSS.III/3, Nairobi.

Van Genderen, J.L. and Lock, B.F., 1977. Testing land-use map accuracy. *Photogrammetric Engineering and Remote Sensing.* 43, 1135-1137.

Van Genderen, J.L., Lock, B.F. and Vass, P., 1978. Remote Sensing: Statistical Testing of Thematic Map Accuracy. *Remote Sensing of Environment.* 7, 3-14.

Walker, A.S., 1982. Deserts in China. *American Scientist.* 70, 366-376.

Walls, J. (ed.), 1982. Combating Desertification in China. *UNEP Reports and Proceedings series 3.*

Zhu, Z. and Liu, S., 1983. *Combating desertification in arid and semi-arid zones in China.* Institute of desert research, Academia Sinica, Lanzhou, China.

Zhu, Z., 1984. The principles and methods for compiling the map of desertification of China. *Journal of Desert Research*, Vol. 4, No.1, Lanzhou, 3-15.

Zhu, Z., Liu, S., Wu, Z. and Di, X., 1986. *Deserts in China,* Institute of Desert Research. Academia Sinica, Lanzhou.

Zhu, Z., Zou, B., Di, X., Wang, K., Chen, G. and Zhang, J., 1988a. *Desertification and Rehabilitation - Case Study in Horqin Sandy Land.* Institute of Desert Research. Academia Sinica, Lanzhou.

Zhu, Z., Liu, S. and Di, X.M., 1988b. *Desertification and Rehabilitation in China.*, ICERDC. Lanzhou, 222p.

Zhu, Z. and Chen, G., 1994. *Sandy Desertification in China.* Press of Science, China, 250p.

MANUALS USED (NOT REFERRED TO)

ESRI, 1991. PC ARC/INFO STARTER KIT, User's Guide. Version 3.4 D Plus.

ESRI, 1991. PC ARCEDIT, User's Guide. Version 3.4 D Plus.

PCI, 1994. Using PCI Software Volume I & II. Version 5.3.

PCI, 1994. GCP Works. Version 5.3.

MAPS

Map of Land Desertification in Horqin Grassland Grassland, 1:500,000, Lanzhou Institute of Desert Research, Academia Sinica, 1991. Chengdu Cartographic Publishing House.

The Map of the Statue of Desertification in Horqin Sandy Land. 1:500,000, Institute of Desert Research, Academia Sinica. Zhonghua Printing House, Shanghai.

PERSONAL COMMUNICATION / UNPUBLISHED PAPERS

Wang, T., Imagawa, T., Methods Applied for Monitoring and Assessing the Sandy Desertification in the North China.

Zhao, Xueyong. Institute of Desert Research, Chinese Academy of Science, 730000 Lanzhou, China.

Lunds Universitets Naturgeografiska institution. Seminarieuppsatser. Uppsatserna finns tillgängliga på Naturgeografiska institutionens bibliotek, Sölvegatan 13, 223 62 LUND.

The reports are available at the Geo-Library, Department of Physical Geography, University of Lund, Sölvegatan 13, S-223 62 Lund, Sweden.

1. Pilesjö, P. (1985): Metoder för morfometrisk analys av kustområden.
2. Ahlström, K. & Bergman, A. (1986): Kartering av erosionskänsliga områden i Ringsjöbygden.
3. Huseid, A. (1986): Stormfällning och dess orsakssamband, Söderåsen, Skåne.
4. Sandstedt, P. & Wällstedt, B. (1986): Krankesjön under ytan - en naturgeografisk beskrivning.
5. Johansson, K. (1986): En lokalklimatisk temperaturstudie på Kungsmarken, öster om Lund.
6. Estgren, C. (1987): Isälvsstråket Djurfälla-Flädermo, norr om Motala.
7. Lindgren, E. & Runnström, M. (1987): En objektiv metod för att bestämma läplanteringars läverkan.
8. Hansson, R. (1987): Studie av frekvensstyrd filtringsmetod för att segmentera satellitbilder, med försök på Landsat TM-data över ett skogsområde i S. Norrland.
9. Matthiesen, N. & Snäll, M. (1988): Temperatur och himmelsexponering i gator: Resultat av mätningar i Malmö.
10A. Nilsson, S. (1988): Veberöd. En beskrivning av samhällets och bygdens utbyggnad och utveckling från början av 1800-talet till vår tid.
10B. Nillson, G., 1988: Isförhållande i södra Öresund.
11. Tunving, E. (1989): Översvämning i Murciaprovinsen, sydöstra Spanien, november 1987.
12. Glave, S. (1989): Termiska studier i Malmö med värmebilder och konventionell mätutrustning.
13. Mjölbo, Y. (1989): Landskapsförändringen - hur skall den övervakas?
14. Finnander, M-L. (1989): Vädrets betydelse för snöavsmältningen i Tarfaladalen.
15. Ardö, J. (1989): Samband mellan Landsat TM-data och skogliga beståndsdata på avdelningsnivå.
16. Mikaelsson, E. (1989): Byskeälvens dalgång inom Västerbottens län. Geomorfologisk karta, beskrivning och naturvärdesbedömning.
17. Nhilen, C. (1990): Bilavgaser i gatumiljö och deras beroende av vädret. Litteraturstudier och mätning med DOAS vid motortrafikled i Umeå.
18. Brasjö, C. (1990): Geometrisk korrektion av NOAA AVHRR-data.
19. Erlandsson, R. (1991): Vägbanetemperaturer i Lund.
20. Arheimer, B. (1991): Näringsläckage från åkermark inom Brååns dräneringsområde. Lokalisering och åtgärdsförslag.
21. Andersson, G. (1991): En studie av transversalmoräner i västra Småland.
22A. Skillius, Å., (1991): Water havesting in Bakul, Senegal.
22B. Persson, P. (1991): Satellitdata för övervakning av höstsådda rapsfält i Skåne.
23. Michelson, D. (1991): Land Use Mapping of theThat Luang - Salakham Wetland, Lao PDR, Using Landsat TM-Data.
24. Malmberg, U. (1991): En jämförelse mellan SPOT- och Landsatdata för vegetations-klassning i Småland.
25. Mossberg, M. & Pettersson, G. (1991): A Study of Infiltration Capacity in a Semiarid Environment, Mberengwa District, Zimbabwe.
26. Theander, T. (1992): Avfallsupplag i Malmöhus län. Dränering och miljöpåverkan.
27. Osaengius, S. (1992): Stranderosion vid Löderups strandbad.
28. Olsson, K. (1992): Sea Ice Dynamics in Time and Space. Based on upward looking sonar, satellite images and a time series of digital ice charts.
29. Larsson, K. (1993): Gully Erosion from Road Drainage in the Kenyan Highlands. A Study of Aerial Photo Interpreted Factors.
30. Richardson, C. (1993): Nischbildningsprocesser - en fältstudie vid Passglaciären, Kebnekaise.

31. Martinsson, L. (1994): Detection of Forest Change in Sumava Mountains, Czech Republic Using Remotely Sensed Data.
32. Klintenberg, P. (1995): The Vegetation Distribution in the Kärkevagge Valley.
33. Hese, S. (1995): Forest Damage Assessment in the Black Triangle area using Landsat TM, MSS and Forest Inventory data.
34. Josefsson, T. och Mårtensson, I. (1995). A vegetation map and a Digital Elevation Model over the Kapp Linné area, Svalbard -with analyses of the vertical and horizontal distribution of the vegetation
35. Brogaard, S och Falkenström, H. (1995). Assessing salinization, sand encroachment and expanding urban areas in the Nile Valley using Landsat MSS data.
36. Krantz, M. (1995): GIS som hjälpmedel vid växtskyddsrådgivning.
37. Lindegård, P. (1996). VINTERKLIMAT OCH VÅRBAKSLAG, Lufttemperatur och kådflödessjuka hos gran i södra Sverige.
38. Bremborg, P. (1996). Desertification mapping of Horqin Sandy Land, Inner Mongolia, by means of remote sensing.